FORUM GEOGRAFI
ISSN: 0852-0682 | E-ISSN: 2460-3945

HTTPS://JOURNALS.UMS.AC.ID/INDEX.PHP/FG/

Research article

Multi-decadal Shoreline Change and Salt Production Exposure in Cirebon, Indonesia: A Cloud Geospatial and Transect-Based Analysis (1995–2025)

Anang Widhi Nirwansyah[1,2*], Dimara Kusuma Hakim[3], Ana Andriani[2], Ismail Demirdag[4], Shreema Rana[5]

[1] Department of Geography Education, Faculty of Education, Universitas Muhammadiyah Purwokerto, Banyumas 53182, Indonesia; [2] Social Science Department, Graduates School of Universitas Muhammadiyah Purwokerto, Banyumas 53182, Indonesia; [3] Department of Informatic Engineering, Faculty of Engineering and Science, Universitas Muhammadiyah Purwokerto Indonesia; [4] City and Regional Planning Department, Atatürk University, Erzurum, Turkey; [5] Faculty of Environment and Resource Studies, Mahidol University, Thailand.

[*)] Correspondence: anangwidi@ump.ac.id

Citation:
Nirwansyah, A. W., Hakim, D. K., Andriani, A., Demirdag, I., & Rana, S. (2026). Multi-decadal Shoreline Change and Salt Production Exposure in Cirebon, Indonesia: A Cloud Geospatial and Transect-Based Analysis (1995–2025). Forum Geografi. 40(2), 244-259.

Article history:
Received: 30 March 2026
Revised: 25 May 2026
Accepted: 25 may 2026
Published: 30 May 2026

Abstract

Coastal salt farming in the Global South is mainly situated in in low-lying intertidal plains, where shoreline migration and morphodynamic variability can quickly manifest as a loss of productive space and disruption of salt-pan infrastructure. In this study, we quantify multi-decadal shoreline change along the Indonesian Cirebon coast during the period 1995–2025 and delineate critical exposure corri-dors where either shoreline retreat or progradation is most likely to cross-cut salt-pan systems, marking areas of intense shoreline mobility and geomorphologic instability. These represent zones of increased rather than direct inundation risk, where shoreline retreat (or progradation) is most likely to cross-cut salt-pan systems. Repeatable geospatial workflow integrated cloud-based multi-temporal optical satel-lite processing was employed, together with transect-based shoreline-change statistics, in order to de-rive the End Point Rate, Linear Regression Rate, Net Shoreline Movement and Shoreline Change Enve-lope within an uncertainty-aware stability framework. Transect classifications are based more on net accretion than net erosion by count, but show a very skewed magnitude distribution, such that local-ized retreat displays larger absolute extremes compared with progradation, yielding slightly negative mean values despite positive medians. Alongshore stratification (west–central–east) indicates that ex-treme values of cumulative displacement and rate are concentrated in the eastern sector, whereas smaller magnitudes and more stable central tendencies are present along the western and central sec-tors. The shoreline changes scale is strongly correlated with the total displacement magnitude, suggest-ing that segments with maximum mobility also show broad positional ranges, as predicted by clustered landscape hotspots. Category-based interpretation adopts these metric signatures and converts them into classes of salt-farming exposure, allowing for a spatially explicit basis for prioritization of parcel overlays, field verification and adaptation planning throughout high-change corridors. The findings advocate hotspot-oriented coastal risk management and the use of geospatial decision support tools for livelihood-sensitive coastal production landscapes.

Keywords: shoreline change; salt production; cloud geospatial analysis; transect-based shoreline metrics; remote sensing; Geographic Information System.

1. Introduction

Coastal socio-ecological systems (SES) in the Global South are increasingly exposed to overlapping pressures from shoreline change, anthropogenic land-use intensification and natural hazards, including episodic events such as flooding and tsunamis (Anugrah & Setiawati, 2022; Cai *et al.,* 2021; Dewa *et al.,* 2023; Liang & Zhou, 2022), as well as persistent processes such as land subsidence (Bramanto *et al.,* 2023; Illigner *et al.,* 2021; Yuwono *et al.,* 2024). These pressures directly threaten coastal livelihoods that depend on stable land-water interactions. Previous studies have shown that terrestrial and coastal food-production systems are vulnerable to sea-level rise, tidal inundation, and salinity change, particularly through the inundation of rice paddies (Glavan *et al.,* 2020) and the salinization or degradation of aquaculture systems (Jayanthi *et al.,* 2022; Nirwansyah & Braun, 2019; Sutrisno *et al.,* 2021). However, traditional salt-farming systems remain comparatively overlooked, despite their strong dependence on stable intertidal landforms, controlled seawater intake, solar evaporation, embankment integrity, and predictable dry-season conditions. While previous research has examined the economic implications of salt yield variability and regional market stability (Nirwansyah *et al.,* 2022; Nirwansyah & Braun, 2021a), less attention has been paid to the proximal hydro-oceanographic and geomorphic processes that physically reshape salt-pan infrastructure. These processes include shoreline retreat, sediment redistribution, longshore sediment transport, wave-energy exposure, tidal-regime shifts, and landform instability, all of which are central to understanding coastal stability and salt-farming exposure (Mageswaran *et al.,* 2021; Pelckmans e*t al.,* 2023; van Bijsterveldt *et al.,* 2022; van Hespen *et al.,* 2023). As a result, the mechanistic basis linking shoreline dynamics to salt-farming vulnerability remains insufficiently developed, limiting the ability to design anticipatory management strategies for this labor-intensive coastal livelihood sector (Wang *et al.,* 2023).

Although coastal vulnerability in the Global South has been widely examined in relation to rice production (Kantamaneni *et al.,* 2020; Salik *et al.,* 2015), aquaculture (Adnan *et al.,* 2020), settlements (Baig *et al.,* 2021) and coastal infrastructure (Islam & Raja, 2021), salt farming has received comparatively less sector-specific attention. This gap is important because salt farming differs from other coastal production systems as it is exposed to shoreline dynamics. Rice farming is commonly affected through salinity intrusion (Hossain *et al.,* 2020), tidal flooding, freshwater scarcity and irrigation disruption, while aquaculture is often assessed through pond inundation (Rutkayová *et al.,* 2018), water-quality degradation, disease risk and salinity fluctuation. Salt farming, by contrast, depends on a narrow balance between stable intertidal land, controlled seawater intake, functional embankments, pond drainage and dry-season solar evaporation (Nirwansyah & Braun, 2021a). As a result, both shoreline retreat and excessive accretion may create operational risks: erosion can remove or fragment salt pans and weaken embankments, whereas accretion can increase sedimentation, obstruct intake channels, alter drainage and raise maintenance needs (Nirwansyah & Braun, 2021b). Therefore, salt-farming vulnerability cannot be fully inferred from frameworks developed for rice or aquaculture, and requires a specific analytical approach that links shoreline dynamics with production-relevant exposure pathways.

Salt production through solar evaporation in intertidal pans is an important socio-economic activity in many coastal areas of the Global South, providing both a food resource and a source of income for coastal communities. Unlike other coastal production systems, salt farming depends on a narrow set of physical conditions: stable pond surfaces, controlled seawater intake, functional embankments, predictable dry-season evaporation and reliable drainage. These conditions are being increasingly disrupted by the combined effects of short-term hazards, such as extreme storms and episodic flooding, and long-term coastal processes, including eustatic sea-level rise, tidal inundation, sediment redistribution and accelerated land subsidence (Bagheri-Gavkosh *et al.,* 2021; Yuwono *et al.,* 2024). In Southeast Asia, such pressures have reduced coastal agricultural productivity and contributed to the physical destabilization of salt-farming infrastructure, including lower yields, pond fragmentation, embankment damage and failure of evaporation ponds (Jayanthi *et al.,* 2022; Nirwansyah & Braun, 2021b). However, despite the growing exposure of salt-farming landscapes, the specific effects of shoreline dynamics on salt production remain insufficiently examined using advanced geospatial approaches (Pantusa e*t al.,* 2022; Zoysa *et al.,* 2023). This gap is significant, because shoreline retreat, accretion and changes in coastal sediment movement may affect salt-pan viability through different mechanisms, including land loss, sedimentation, altered seawater access, increased maintenance needs and reduced operational reliability. Recent studies on digital and infrastructure monitoring highlight the broader importance of data-supported approaches for improving resilience assessment, operational decision-making and anticipatory management of exposed infrastructure systems (Phan & Stive, 2022; Wang *et al.,* 2023). In this study, we extend this logic to a coastal livelihood setting by using shoreline-change analysis to translate coastal morphodynamics into operationally meaningful information for salt-farming adaptation. Consequently, the study examines how combined natural and anthropogenic forces are shaping shoreline dynamics and salt-farming exposure in the coastal landscape of Cirebon, West Java, Indonesia.

Understanding the hydro-oceanographic and geomorphic processes that govern shoreline change is essential for explaining how coastal dynamics affect salt-farming systems. Shoreline evolution is shaped by interacting processes operating across different temporal and spatial scales, including wave energy, tidal range and frequency, longshore currents, sediment transport, extreme weather events, cyclones, and storm surges (Al-Ali *et al.,* 2024; Jayanthi *et al.,* 2022; Kumar *et al.,* 2021; Makris *et al.,* 2023; Tang *et al.,* 2023). Wave action, for example, can drive sediment redistribution and contribute to both erosion and accretion, thereby altering the position and stability of the shoreline (Gallina *et al.,* 2020; Jayanthi *et al.,* 2023; Solihuddin *et al.,* 2021; Wisha *et al.,* 2022). Tidal dynamics are equally important for salt farming because tidal range, inundation frequency and seawater circulation influence the exposure of salt pans, the reliability of seawater intake, pond drainage, evaporation conditions, and the timing of salt production (Dewi & Bijker, 2020; Pantusa *et al.,* 2022; Phan & Stive, 2022). However, previous studies have rarely integrated these physical drivers into a cohesive framework that explains how shoreline retreat, accretion, sedimentation and tidal exposure translate into operational risks for salt farming salinas and salt-pan infrastructure (Nirwansyah *et al.,* 2023; Pantusa *et al.,* 2022; Zoysa *et al.,* 2023). This lack of integration limits the ability to move from shoreline-change measurement toward a mechanistic understanding of salt-farming vulnerability.

Determining the different hydro-oceanographic processes that govern coastal change is one of the main challenges in studying shoreline dynamics. These multi-temporal and spatially acting processes are related to wave energy, tidal frequency and longshore currents, together with extreme

weather events such as cyclones and storm surges (Al-Ali *et al.,* 2024; Jayanthi *et al.,* 2022; Kumar *et al.,* 2021; Makris *et al.,* 2023; Tang *et al.,* 2023). Wave action, for instance, is a significant factor affecting the shoreline by enabling sediment transport and causing both erosion and accretion (Gallina *et al.,* 2020; Jayanthi *et al.,* 2023; Solihuddin *et al.,* 2021; Wisha *et al.,* 2022). Likewise, the aforementioned tidal dynamics, including both tidal range and inundation patterns, play a major role in modulating the exposure of salt pans to seawater and markedly affects evaporation rates and the overall salt production process (Dewi & Bijker, 2020; Pantusa *et al.,* 2022; Phan & Stive, 2022). Despite the strong links, past studies have rarely integrated these aspects into a cohesive framework that thoroughly explains how any physically relate to shorelines adjacent to salinas in the context of salt production (e.g. Nirwansyah *et al.,* 2023; Pantusa *et al.,* 2022; Zoysa *et al.,* 2023).

There is a growing realization in the scientific community that we need to leverage remote sensing data and geospatial analysis in order to monitor shoreline changes. Long-term observations of shoreline shift can be acquired remotely and data from sensors deployed on platforms such as Landsat and Sentinel-1 have been proven to provide high temporal and spatial resolution products (Elnabwy *et al.,* 2020; McClenachan *et al.,* 2020; Muskananfola *et al.,* 2020; Zoysa *et al.,* 2023). Complemented by ground-based observations and socio-economic information, these types of data provide a comprehensive view of how shoreline dynamics impact local communities. Shoreline changes, including End Point Rate (EPR), Linear Regression Rate (LRR) and Net Shoreline Movement (NSM) parameters, have been quantified successfully using Geographic Information System (GIS)-based Digital Shoreline Analysis Systems (DSAS). These have now become a routine process since the DSAS algorithm is widely available to researchers in its current versions, such as DSAS v4, for shoreline change assessment on regional and global scales over time with statistical accuracy (Abd-Elhamid *et al.,* 2023; Ciritci & Türk, 2019; Gallina *et al.,* 2020; Pantusa *et al.,* 2022; Wisha *et al.,* 2022). Use of these methodologies in salt farming regions can generate high-resolution vulnerability maps that allow definition of the areas at higher risk of erosion and inundation. Such approaches have been supported by recent developments on cloud-based geospatial platforms; for example, Google Earth Engine (GEE) applications for environmental monitoring of coastal ecosystem variables, including mangroves and seagrasses (Huang *et al.,* 2025; Lizcano-Sandoval *et al.,* 2022; Meister & Qu, 2024; Traganos *et al.,* 2018).

However, there remains a lack of examination of the impacts in relation to shoreline dynamics and salt production in the Global South, especially Southeast Asia, despite advances in shoreline monitoring techniques (Baig *et al.,* 2021; Fathurrahman *et al.,* 2025). While several studies have focused on broader economic losses in agriculture or aquaculture (Chung *et al.,* 2019; Rutkayová *et al.,* 2018; Shokoohi *et al.,* 2018), salt farming systems specifically have received relatively little attention. In addition, studies have relied on overly simplistic models to measure the impacts of shoreline change, which may seriously understate the dangers posed to coastal communities and salt production infrastructure (Dhanalakshmi *et al.,* 2019; Ekrami *et al.,* 2021; Stelten & Antczak, 2022; Susantoro *et al.,* 2020). In this regard, our study intends to improve on previous research by using advanced geospatial techniques that allow for quantification of both the direct and indirect effects of shoreline dynamics on salt farming in Cirebon, hence providing updated understanding of the complex interplay between human development and natural processes. Consequently, the work intends to improve on previous studies by describing the mechanistic connection between hydro-oceanographic-induced shoreline morphodynamics and the recent viability of classical salt production in Cirebon, West Java.

Utilizing a high-resolution, multi-decadal RS-GIS framework that integrates the Google Earth Engine (GEE) cloud-processing platform and the QGIS Shoreline Change Analysis Tool (QSCAT), the research makes two specific contributions. First, we quantify net shoreline displacement and estimate multi-decadal (1995–2025) linear regression rates to ensure high levels of planimetric accuracy. Second, we identify and map critical vulnerability zones where shoreline retreat or accretion intersects with salt-pan infrastructure. Ultimately, these advanced geospatial techniques will allow for the quantification of both direct and indirect effects of shoreline dynamics, providing updated understanding of the complex interplay between human development and natural processes.

2. Methods

Using a comprehensive geospatial approach, the study aims to investigate shoreline dynamics and their impacts on salt production in Cirebon, West Java, Indonesia. The methodology incorporates data gathered through remote sensing, numerical model outputs and geospatial information (GIS) tools, permitting systematic and quantitative evaluation of shoreline morphodynamics, together with assessment of how the dynamics relate to salt production areas (as illustrated in Figure 1).

The study seeks to generate better understanding how such shoreline dynamics influence salt farming activities by integrating different geospatial tools, thus resulting in a robust decision pathway towards sustainable coastal management and adaptation. Details of the research process are provided in the following sub-sections.

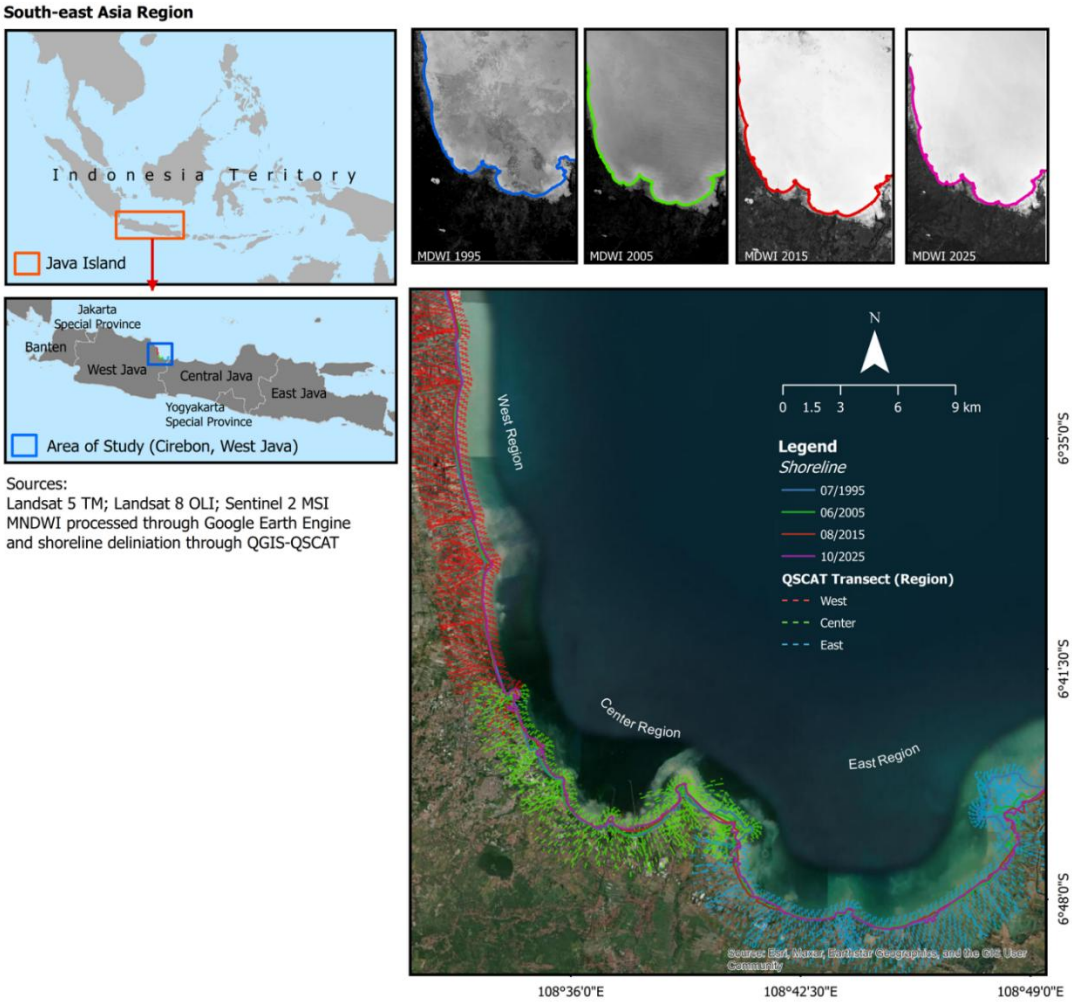

Figure 1. Geographic Setting of the Cirebon Coastline and Multi-Temporal Shorelines (1995–2025) Extracted Using MNDWI and Analyzed with QGIS–QSCAT Transects.

2.1. Satellite Data Acquisition

Three decades of shoreline evolution were captured from a multi-sensor longitudinal dataset consisting of four temporal snapshots from 1995, 2005, 2015 and 2025. These decadal epochs were selected to capture long-term shoreline evolution, while maintaining temporal consistency across the multi-sensor dataset. Data were accessed and processed in the Google Earth Engine (GEE) cloud-computing environment. The 1995 and 2005 epochs were constructed using Landsat 5 Thematic Mapper (TM) Surface Reflectance (SR) data, while the 2015 epoch used Landsat 8 Operational Land Imager (OLI) SR data, and the 2025 snapshot employed Sentinel-2 Multi-Spectral Instrument (MSI) Level-2A Bottom-of-Atmosphere products (Table 1). The use of decadal snapshots reflects a trade-off between temporal frequency and the need for consistent image quality, shoreline visibility and sufficient spatial detail in a tropical coastal environment where cloud cover, haze, vegetation and tidal-stage variability can complicate shoreline interpretation vegetation (Anderson *et al.,* 2021; Chakma & Akter, 2021; Dewi & Bijker, 2020; Jayanthi *et al.,* 2023; Makris *et al.,* 2023). Intermediate years between 2015 and 2025 were not included in the main analysis because the study was designed to assess net decadal shoreline change rather than annual or event-scale variability. Therefore, the 2015–2025 period should be interpreted as one of net change, and shorter-term fluctuations within that decade may not be fully captured.

To minimize cloud contamination, candidate images for each target year were filtered in Google Earth Engine using image-level cloud-cover metadata. Landsat 5 TM and Landsat 8 OLI Surface Reflectance scenes were filtered using the CLOUD_COVER metadata property, while Sentinel-2 MSI Level-2A scenes were filtered using the CLOUDY_PIXEL_PERCENTAGE metadata property. For all sensors, only images with reported cloud cover of ≤10% were retained. This

procedure was used as a scene-level screening step rather than a pixel-level quality-assessment masking procedure. All the retained images were visually inspected to ensure that the shoreline and adjacent salt-farming areas were not obscured by residual cloud, cloud shadow, haze or other atmospheric artefacts. Images with visible obstruction over the coastline or salt-pan areas were excluded from the final composite.

For each target year (see Table 1), the retained images were composited using a median reducer. The median composite was used to reduce the influence of short-term atmospheric noise, residual cloud contamination and spectral outliers. This approach produced cloud-minimized annual composites for shoreline interpretation, while maintaining a transparent and reproducible image-selection procedure across all target years. This multi-platform factor allowed the study to take advantage of both optical and radar remote sensing for consistent monitoring, which is challenging in a tropical climate such as that of the Cirebon region (Abd-Elhamid *et al.,* 2023; Gómez-Pazo *et al.,* 2021). In addition, a median-reducer algorithm was implemented for the collection of images for each target year in order to yield a cloud-free composite, effectively minimizing transient atmosphere noise and outliers. To enable planimetric accuracy and ensure spatial integrity during the quantitative analysis of the region, all the spatial data were projected into the Universal Transverse Mercator (UTM) Zone 49S coordinate system.

Table 1. Multi-Source Satellite Data Required for the Study.

Year	Satellite	Number of Bands	Spatial Resolution	Date	References
1995	Landsat 5 TM	7	30 meters	July 1995	Chander *et al.* (2007, 2009)
2005	Landsat 5 TM	7	30 meters	June 2005	Chander *et al.* (2007, 2009)
2015	Landsat 8 OLI	11	30 meters	August 2015	Roy *et al.* (2026); Zhang and Roy (2016)
2025	Sentinel-2 MSI	13	10, 20, 60 meters	October 2025	Dewi and Bijker (2020); Muskananfola *et al.* (2020)

2.1.1. Shoreline Extraction and Baseline Development

Satellite images require preprocessing before shoreline extraction to ensure spatial consistency, radiometric comparability and reliable water-land discrimination (Bushra *et al.,* 2021; Shamsuzzoha & Ahamed, 2023; Yulfa *et al.,* 2022). In this study, preprocessing involved image selection, cloud-screening, geometric consistency checking, spectral-index calculation and shoreline vector refinement. Water-land boundaries were initially identified using the Modified Normalized Difference Water Index (MNDWI), which is widely employed for separating water features from land surfaces in coastal environments (Elnabwy *et al.,* 2020; Shamsuzzoha & Ahamed, 2023). The MNDWI was selected because it improves the spectral contrast between open water and surrounding land-cover types by using the green and short-wave infrared bands. This is particularly useful in coastal salt-farming landscapes, where salt-pan surfaces, shallow inundation, built-up areas and exposed sediment may interfere with standard water detection (Al-Ali *et al.,* 2024; Yulfa *et al.,* 2022).

The MNDWI was calculated using sensor-specific green and SWIR1 bands. For Landsat 5 TM, Band 2 and Band 5 were used; for Landsat 8 OLI, Band 3 and Band 6 were used; and for Sentinel-2 MSI, Band 3 and Band 11 were used. The formulations are shown in Table 2. Because Sentinel-2 Band 11 has a native spatial resolution of 20 m, it was resampled to 10 m using bilinear interpolation to match the spatial resolution of the visible bands before index calculation. This ensured consistency between the green and SWIR inputs used for the MNDWI-based shoreline extraction.

The resulting MNDWI raster was classified using a binary threshold to separate water and non-water pixels, with positive MNDWI values interpreted as water, and negative ones as land. The resulting water-land masks were then converted into vector polylines to generate preliminary shoreline boundaries. These vector shorelines were subsequently checked and refined to remove artefacts caused by isolated pond inundation, floating materials, vegetation edges or spectral confusion between shallow water and exposed salt-pan surfaces. The refined vectors were then used as the baseline input for the multi-decadal shoreline-change analysis.

Table 2. Modified Normalized Difference Water Index (MNDWI) Band Formulations by Satellite Sensor.

Satellite	MDWI equation	
Landsat 5 TM	$\frac{\text{Band2(Green)} - \text{Band5(SWIR1)}}{\text{Band2(Green)} + \text{Band5(SWIR1)}}$	(1)
Landsat 8 OLI	$\frac{\text{Band3(Green)} - \text{Band6(SWIR1)}}{\text{Band3(Green)} + \text{Band6(SWIR1)}}$	(2)
Sentinel-2 MSI	$\frac{\text{Band3(Green)} - \text{Band11(SWIR1)}}{\text{Band3(Green)} + \text{Band11(SWIR1)}}$	(3)

2.1.2. Tidal Consistency and Shoreline Refinement

The high-water line was selected as the shoreline proxy as it is visually identifiable in optical satellite imagery and provides a consistent indicator for interpreting long-term shoreline movement in the study area. The proxy is also appropriate for coastal settings where historical field-based shoreline records are limited. However, the position of the high-water line can be affected by the tidal stage at the time of satellite acquisition, especially in low-gradient intertidal environments such as salt-farming coasts. As a result, part of the apparent horizontal shoreline displacement may reflect tidal aliasing rather than purely geomorphic change.

Full tidal correction was not applied in the study because consistent tide-level data were not available for all historical satellite acquisition dates across the 1995, 2005, 2015 and 2025 years epochs. Instead, local tidal evidence was used to contextualize the potential influence of tidal-stage variability on shoreline interpretation. Recent radar tide-gauge observations in Cirebon waters show that the area has a mixed prevailing semidiurnal tidal regime, with an approximate tidal range of 0.8–1.0 m (Badriana *et al.,* 2024). Furthermore, high tides commonly occur around 06:00–09:00 and 18:00–21:00 local time, while low tides commonly occur around 11:00–14:00 and 01:00–04:00. These observations indicate that tidal-stage variability may influence the horizontal position of shorelines interpreted from optical imagery, particularly along low-lying salt-pan margins.

After the MNDWI-based shoreline was generated, a semi-automated refinement procedure was employed to improve shoreline consistency. Fully automated edge-detection algorithms, such as the Canny operator, can support rapid shoreline delineation, but may perform less reliably in intertidal salt-pan landscapes with complex spectral signatures (Yasir *et al.,* 2020). Therefore, supervised morphological delineation was used as a quality-control step to refine the final shoreline vectors. This process helped remove transient spectral noise caused by localized pond inundation, shallow water, floating debris and mixed land-water pixels. Such refinement improves the planimetric consistency of shoreline vectors and provides a more reliable input for multi-decadal shoreline-change analysis (Gómez-Pazo *et al.,* 2021).

2.2. Geostatistical Shoreline Analysis

Quantitative analysis of shoreline evolution was performed using the QGIS Shoreline Change Analysis Tool (QSCAT), which enables systematic calculation of shoreline displacement and shoreline-change statistics from multi-temporal shoreline vectors (Facun *et al.,* 2025; Galan *et al.,* 2026; Manurung et al., 2025). An offshore baseline was constructed following the general orientation of the Cirebon coastline, and orthogonal transects were generated at fixed 50 m intervals. In total, 668 transects were used in the analysis, with transect numbering starting from the westernmost section and increasing eastward from Transect 1 to Transect 668. For spatial interpretation, the transects were divided into three coastal segments: west coast, transects 1–223; central coast, transects 224–445; and east coast, transects 446–668. The transects were generated with a length of 3,000 m to ensure intersection with all shoreline positions across the 1995, 2005, 2015 and 2025. The baseline was smoothed using a 500 m window to reduce geometric artefacts caused by localized shoreline irregularities and to improve transect-orientation consistency. Net Shoreline Movement (NSM) and End Point Rate (EPR) were calculated for each transect to quantify the magnitude and rate of shoreline displacement over the study period.

To account for positional and processing uncertainty, an uncertainty budget was incorporated into the QSCAT workflow. Because field-based shoreline error measurements were unavailable for the historical epochs, the uncertainty values were adopted as pragmatic processing parameters rather than site-specific field-validated error estimates. A shoreline uncertainty value of 25 m and a QSCAT-specific processing uncertainty, qs_uncer, of 15 m were applied consistently across all shoreline epochs and transects. The 25 m shoreline uncertainty was considered reasonable for this multi-sensor analysis because it is broadly comparable to the spatial scale of the Landsat-based epochs and accounts for uncertainty related to sensor resolution, possible co-registration differences, mixed land-water pixels, high-water-line interpretation, and tidal-stage variability. These sources of uncertainty are commonly recognized in optical shoreline extraction and multi-temporal shoreline-change analysis (Apostolopoulos & Nikolakopoulos, 2020; Dewidar & Bayoumi, 2021; Sunny *et al.,* 2022). The 15 m qs_uncer parameter was used to represent additional uncertainty associated with shoreline delineation and transect-intersection processes during QSCAT calculation. These values should not be interpreted as field-validated positional errors, but as conservative and consistent uncertainty settings used to support cautious interpretation of shoreline-change statistics, particularly for low-magnitude shoreline changes that may be affected by image resolution, shoreline-proxy ambiguity and tidal-stage variability.

2.3. Classification and Vulnerability Assessment

The geostatistical outputs were then grouped according to their morphodynamical trends and relevant risks to assess the implications of shoreline evolution for salt-production feasibility. A classification framework of four regions is proposed based on global vector models of Shoreline Change Envelope (SCE), Net Shoreline Movement (NSM) and End Point Rate (EPR), adjusted accordingly. NSM is signed (negative = retreat; positive = progradation) and SCE is unsigned in this case. Therefore, analyses linking SCE with cumulative displacement employed |NSM| in comparisons of magnitude and signed NSM in classifications of erosion–accretion. This transformation was made only to compare magnitudes with SCE; signed NSM was preserved to facilitate directional interpretation across results. Moreover, landward accretionary trends were grouped into three classes: stable accretion rate, moderate accretion rate, and high chance for the amelioration of a high chance of improved progress. Using these categories, we assessed the "coastal distance" challenge of excessive land growth that potentially decouples salt-pan infrastructure from seawater intake over time in a timely fashion. In contrast, zones showing negative long-term displacement or landward migration were categorized as at risk of inundation. In these high-vulnerability areas, Weighted Linear Regression (WLR) was selected as the key indicator to derive trends for at-risk land submergence over the long term, and for permanent loss of land. All rates were assessed at a 95% confidence interval, meaning that resultant retreat/accretion rates across the Cirebon salt-production landscape are significant and represent true geomorphological trends. Notably, this coupled assessment enabled the linkage of changes to physical shorelines with threats to operational stability in the Cirebon salt-farming sector and thus provided a metric for determining which regions may require urgent adaptive action. The overall research workflow is summarized in Figure 2.

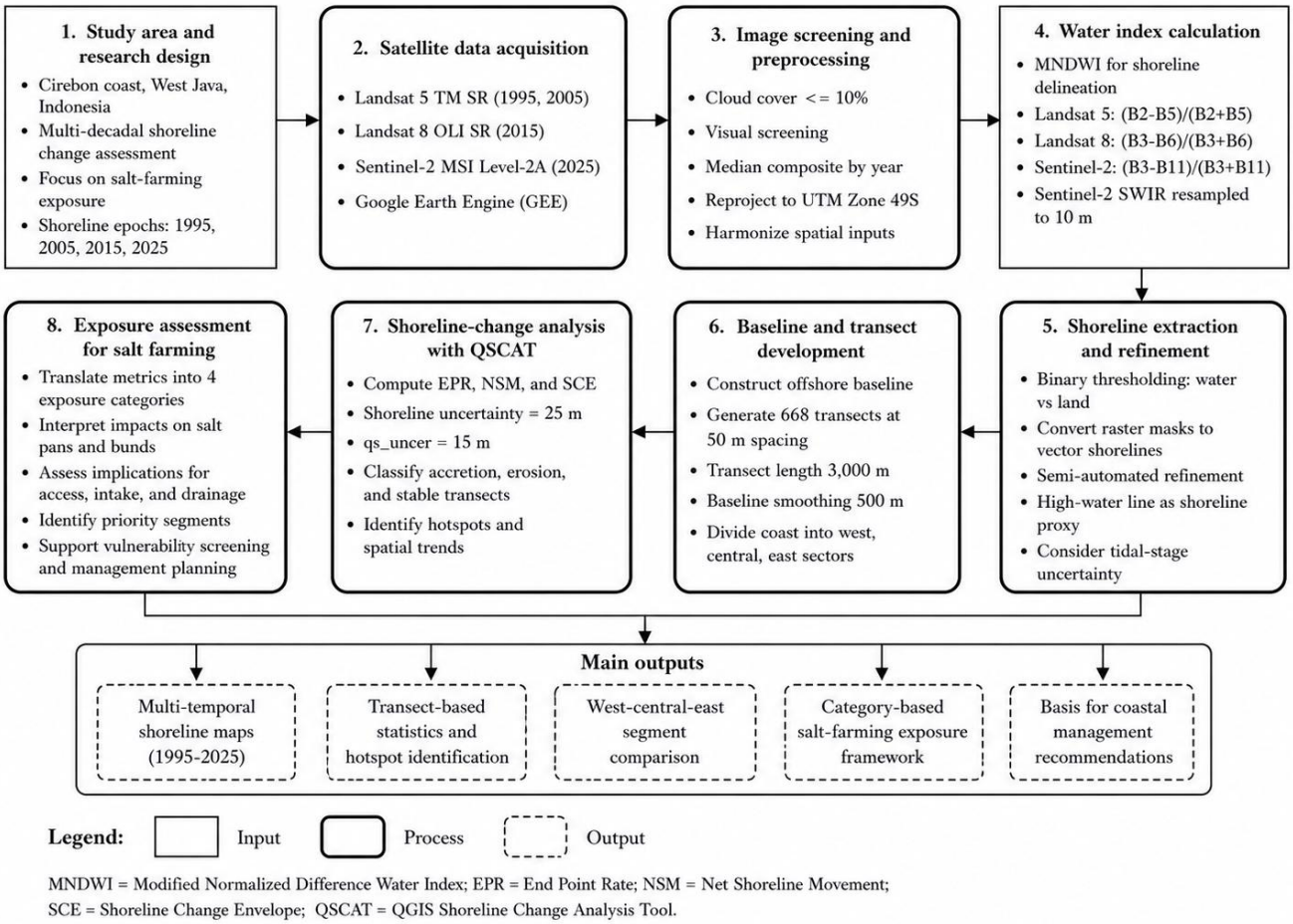

Figure 2. Methodological Framework for Shoreline Extraction, Shoreline-Change Analysis, and Salt-Farming Exposure Assessment.

3. Results and Discussion

To comprehensively address the spatial heterogeneity of the Cirebon coastline, the quantitative metrics in the study are grounded in a series of high-resolution spatial visualizations generated through the integrated GEE and QSCAT workflow. Before detailing the statistical rates of change,

it is critical to establish the overarching spatial context of the study area over the 30-year observation window (1995–2025). The spatial analysis is driven by three primary visual output. First, the multi-temporal shoreline extraction map visually chronicles the decadal shifts in the land-water interface, highlighting macro-level coastal reconfiguration and the formation of localized geomorphic hotspots. Second, transect-based morphodynamic heatmaps (visualizing EPR and NSM distributions, as discussed in subsequent sections) spatially disaggregate the coastline into West, Central, and East sectors. These visualizations are crucial because they reveal that while accretion is statistically dominant by transect count, extreme erosion events are not randomly distributed; rather, they form distinct, spatially coherent clusters. Finally, the visualizations provide a geographic basis for identifying priority areas for salt-farming exposure assessment. By projecting the QSCAT transect data in the GIS, the visualizations transition the data from abstract coastal morphodynamics into applied, category-based vulnerability zones, directly illustrating which salt-farming parcels face imminent landward retreat (erosion) or excessive seaward progradation (sedimentation). Together, they provide the necessary geographic context for interpreting the highly uneven transect statistics detailed in the following sections.

3.1. Shoreline Change Trend (1995-2025)

Shoreline-change assessment in Cirebon is based on the standard shoreline-cover metrics generated from QGIS-QSCAT transect export (n = 668 transects): End Point Rate (EPR, m/year), Linear Regression Rate (LRR, m/year), Net Shoreline Movement (NSM, m) and Shoreline Change Envelope (SCE, m). Overall spatial pattern is directionally mixed (again, accretion dominates erosion by transect count), with highly uneven magnitudes across the coastal expanse; this heterogeneity is reflected in the divergence between mean and median statistics, in which a few extreme erosion sites bring the average down, masking the typical accretionary behavior seen across most of the region. EPR in this research also varies between −81.86 m/year and +59.14 m/year (Figure 3a), while NSM also varies from −2476.28 m to +1789.01 m (shown in Table 3 and Figure 3b). The median ensemble planform retreat (EPR) is positive (+1.83 m/year), as is the median net-shoreline migration (NSM) (+55.33 m), indicating that typical transects undergo seaward displacement, whereas the mean EPR (−0.97 m/year) and mean NSM (−29.38 m) are slightly negative due to a smaller number of extreme erosional segments having disproportionally strong influence. LRR displays a similar distributional structure (median +1.89 m/year; mean −0.78 m/year) (presented in Figure 3c), suggestive of bulk accretionary behavior with concentrated hotspots for ephemeral erosion.

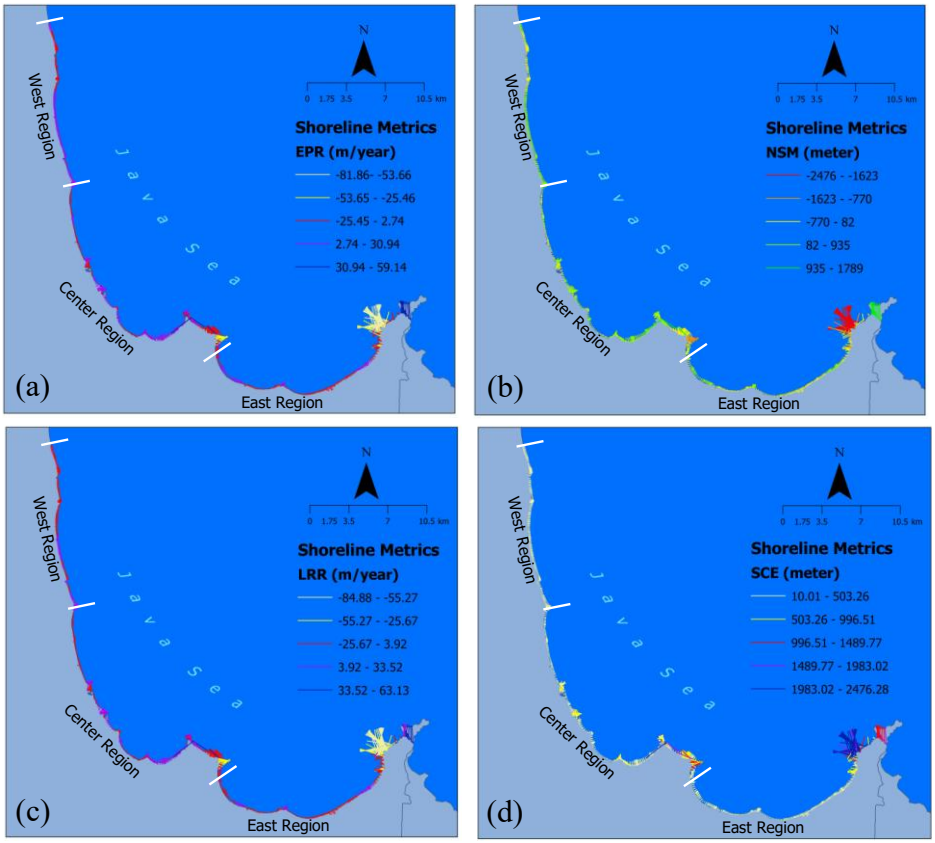

Figure 3. Representation of Shoreline-Change Parameters in Cirebon Between 1995–2025 Based on: a) EPR, b) LRR, c) NSM, and d) SCE.

The SCE, as a non-directional measure of variability in the position of the shoreline, ranges from 10.01 m to 2,476.28 m, with a median value of 170.31 m, and the large upper tail indicating that certain sectors deployed wide positional envelopes throughout the observation window, resulting in pronounced morphodynamic variability (see Figure 3d). In order to interpret how this positional envelope relates to net change, SCE was compared on a per-transect basis against the cumulative displacement magnitude (|NSM|), with SCE unsigned and NSM signed. In relation to the three alongshore divisions created (West: transects 1–223; Central: 224–445; East: 446–668) the relationship between SCE and |NSM| remains consistently positive and strong across each sector ($r \approx 0.83$ in both West and Central sectors, $r \approx 0.97$ in East sector), implying that over displaced transects, larger amounts of shoreline envelopes are also generally representative, with strongest coupling within the eastern segment, where the extreme values of displacement are concentrated (see Figure 4). Another factor raised with respect to interpretation is that of uncertainty handling; the dataset indicates that all transects possess an EPR_unc = 0.70 m/year (for all transects), suggesting that stability may have been defined using some form of uncertainty-based neutral band around zero.

Table 3. Summary of Shoreline-Change Metrics in Cirebon from 1995–2025.

Metric	Min	Max	Mean	Median	Std Dev
EPR (m/year)	-8186	59.14	-0.97	1.83	18.24
NSM (m)	-2,476.28	1,789.01	-29.38	55.33	551.72
LRR (m/year)	-84.88	63.13	-0.78	1.89	17.71
SCE (m)	10.01	2,476.28	353.44	170.31	503.92

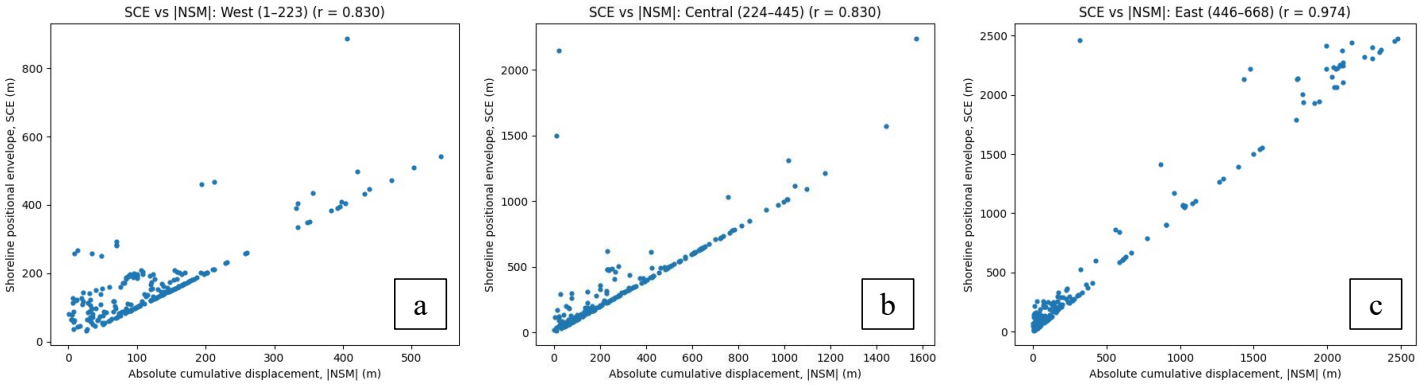

Figure 4. Relationship Between the Shoreline Positional Envelope (SCE) and the Magnitude of Cumulative Shoreline Displacement |NSM| Across Alongshore Sectors of Cirebon.

3.2. Erosion and Accretion (Direction, Magnitude and Hotspots)

The QSCAT trend classification indicates that shoreline accretion is more widespread than erosion when assessed by transect count. Based on the End Point Rate trend classification (EPR_trend), 421 of the 668 transects, or 63.0%, were classified as accreting, while 192, or 28.7%, were eroding, and 55, or 8.2%, were stable. A similar pattern was obtained from the Net Shoreline Movement trend classification (NSM_trend), in which 430 transects, or 64.4%, were accreting, 204, or 30.5%, were eroding, and 34, or 5.1%, were stable (Table 4). The consistency between the EPR and NSM_trends suggests that the dominance of accreting transects is not merely an artefact of a single shoreline-change metric; rather, both indicators show that much of the Cirebon coastline experienced seaward shoreline movement or relative stability during the observation period. Nevertheless, this count-based dominance should not be read as evidence that erosion is negligible, as transect frequency does not capture the magnitude of shoreline retreat at specific locations.

Table 4. Distribution of Shoreline-Change Trend Classes Based on EPR and NSM Across the 668 Cirebon Coastal Transects.

Metric trend class	Accreting	Eroding	Stable
EPR_trend	421 (63.0%)	192 (28.7%)	55 (8.2%)
NSM_trend	430 (64.4%)	204 (30.5%)	34 (5.1%)

However, the dominance of accretion by transect count must be interpreted together with the magnitude and spatial distribution of both the EPR and NSM values. Although most transects were classified as accreting, the magnitude distribution was skewed by a smaller number of high-

erosion ones. This pattern is reflected in the coexistence of positive median values with negative mean values, particularly for NSM, where the median remained positive at +55.33 m, while the mean was negative at −29.38 m. This indicates that the median better represents the more common condition across the coastline, whereas the mean is strongly influenced by localized retreat segments with extreme values. Therefore, negative mean values should not be interpreted as evidence of uniform erosion along the entire Cirebon coast, but rather as an indication of spatially uneven shoreline dynamics and localized erosion hotspots.

Hotspot identification based on EPR further shows that the highest accretion rates occurred at Transects 657 (+59.14 m/year), 387 (+51.96 m/year), 668 (+50.87 m/year), 658 (+49.49 m/year) and 369 (+47.66 m/year), while the highest erosion rates were found at Transects 651 (−81.86 m/year), 650 (−81.20 m/year), 619 (−78.19 m/year), 640 (−77.92 m/year) and 630 (−76.28 m/year) (as presented in Figure 5). The NSM range, from −2476.28 m to +1789.01 m, confirms that the shoreline-change distribution contains a limited number of high-magnitude retreat and advance values. These extreme transects may represent genuine geomorphic hotspots, especially where they form spatially coherent clusters, but they should also be interpreted cautiously because satellite-derived shoreline proxies can be affected by shoreline-extraction uncertainty, tidal-stage variability, mixed land-water pixels, salt-pan inundation, or localized spectral noise. Therefore, the interpretation emphasizes clustered erosion and accretion patterns shown in the segmentation map rather than isolated transect-level extremes.

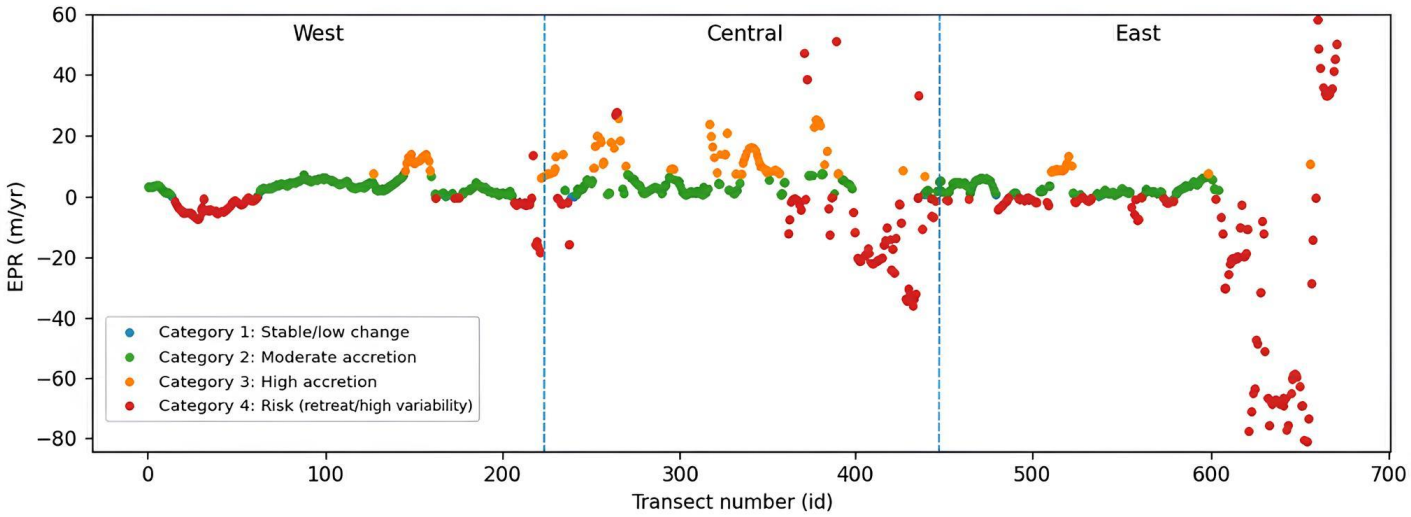

Figure 5. Spatial Distribution of EPR (m/year) Along the Cirebon Shoreline Transects.

3.3. Category-Based Shoreline Change and Implications

QSCAT outputs, including EPR, NSM and SCE, were interpreted using a category-based framework to translate transect-scale shoreline-change metrics into salt-farming exposure classes. Category 1 represents stable or low-change segments, in which EPR falls within the uncertainty-defined neutral band, EPR_unc = 0.70 m/year, and NSM and SCE values remain comparatively low. These segments are interpreted as having relatively high shoreline predictability and lower direct exposure for salt-pan infrastructure. Category 2 represents moderate accretion or seaward displacement beyond the stability threshold, but below the highest observed magnitudes. This condition may indicate gradual shoreline progradation that could require periodic adjustment of seawater-intake alignment, access routes or pond boundaries. Category 3 represents high accretion and/or high-envelope behavior, indicated by strongly positive EPR or NSM values and large SCE magnitudes. Although accretion is often interpreted as land gain, in salt-farming systems excessive accretion can be operationally problematic because it may increase sedimentation, obstruct seawater-intake channels, alter drainage pathways, reduce hydraulic connectivity between ponds and the sea, and require repeated channel maintenance or pond-boundary adjustment.

Category 4 identifies the highest-risk shoreline-instability segments, characterized by landward displacement, negative EPR and/or NSM values, and/or very large SCE values. Because high-resolution elevation, tidal-range and field-based inundation data were unavailable, Category 4 is interpreted as a shoreline-instability exposure proxy rather than a direct inundation-risk zone. Nevertheless, this category is considered highly relevant for salt-pan vulnerability because shoreline retreat may reduce production space, damage pond margins, increase stress on bunds and access routes, and expose intake or drainage infrastructure to more frequent disturbance. Sector-level summaries indicate that the eastern sector, Transects 446–668, contains the most extreme

displacement magnitudes, including both cumulative retreat and rapid progradation, while the western and central sectors show more positive medians and less severe extremes. Therefore, priority areas for higher-resolution salt-pan mapping are those that spatially intersect or immediately adjoin Category 4 transects, followed by Category 3 transects, where rapid accretion or shoreline reconfiguration may impose repeated operational adjustment.

To make the exposure framework less subjective, the expected severity classes were anchored to measurable shoreline-change indicators and operational proxies rather than qualitative judgement alone. These indicators include EPR direction and magnitude, NSM displacement, SCE envelope size, transect location within west-central-east sectors, and spatial proximity or overlap with salt-farming parcels. In this framework, Category 4 is prioritized when negative EPR/NSM and large SCE indicate shoreline retreat or instability near salt-pan infrastructure, while Category 3 is prioritized when high positive EPR/NSM and large SCE suggest rapid accretion that may affect seawater intake, drainage, sediment management and pond access. Because direct data on maintenance costs, intervention frequency or production loss were not available, the severity ranking should be interpreted as an exposure-based prioritization tool rather than a direct economic damage estimate. Table 5 summarizes the expected impact pathways and measurable indicators used to identify potential vulnerability zones where shoreline dynamics intersect with salt-farming infrastructure.

Table 5. Impact Matrix Linking Shoreline-Change Categories to Salt-Farming Implications and Priority for Vulnerability Mapping.

Category	Shoreline-change signature	Expected salt-farming impact	Expected severity	Measurable indicator-/ operational proxy
Category 1	Stable or low-change shoreline; EPR within neutral band; low NSM and SCE	Relatively predictable shoreline position; routine monitoring needed	Low	EPR within EPR_unc; low NSM; low SCE; limited overlap with salt-pan margins
Category 2	Moderate accretion or seaward displacement	Gradual shoreline progradation; possible adjustment of intake alignment, access routes, or pond boundaries	Moderate	Positive EPR/NSM above stability threshold but below high-accretion class; moderate SCE
Category 3	High accretion and/or high SCE	Sedimentation, intake-channel obstruction, drainage alteration, reduced hydraulic connectivity, repeated channel or boundary maintenance	Moderate to high	High positive EPR/NSM; large SCE; overlap or proximity to intake/drainage corridors and salt-pan margins
Category 4	Landward displacement, negative EPR/NSM, and/or very large SCE	Pond loss or fragmentation, bund stress, shoreline retreat near production space, access-route disruption	High	Negative EPR/NSM; large SCE; overlap or adjacency with salt-pan parcels or coastal infrastructure

3.4. Discussion

The results from Cirebon confirm a pattern widely reported for dynamic tropical and Global South coastlines: shoreline behavior is directionally mixed and spatially clustered, where an accretion-dominant transect count can coexist with localized but severe retreat hotspots that strongly influence magnitude-based interpretation. This pattern explains why the mean values may become slightly negative despite positive median values, indicating that a smaller number of high-magnitude erosion transects exert a strong influence on coastline-wide statistics. Similar hotspot-based shoreline dynamics have been reported in multi-decadal studies, with erosion and accretion being shaped by interacting hydro-oceanographic and anthropogenic drivers rather than by uniform shore-wide trends (Gallina *et al.,* 2020; Jayanthi *et al.,* 2023; Mageswaran *et al.,* 2021; Pantusa *et al.,* 2022). The alongshore segmentation in this study further shows that the eastern part of the Cirebon coastline contains the highest extremes, supporting the interpretation that shoreline-change "cells" and modified sediment systems can create adjoining zones of contrasting erosion and accretion (Dewi & Bijker, 2020; Pantusa *et al.,* 2022; Zoysa *et al.,* 2023). When benchmarked against other Indonesian and Southeast Asian coastal studies, this pattern is not unusual. In Quang Nam, Vietnam, DSAS-based analysis found both erosional and accretional transects over the period 1990–2019, with strong localized erosion reaching −42.4 m/year near the Cua Dai estuary (Quang *et al.,* 2021). In East Java, Indonesia, multi-sensor remote-sensing analysis showed that accretion was generally more pronounced than erosion, but some deltaic and aquaculture-mangrove areas experienced very large local shoreline changes, with EPR values ranging from strong erosion to very high accretion (Arjasakusuma *et al.,* 2021). Recent work in the Upper Gulf of Thailand also shows that erosion and accretion can vary strongly across periods and regions due to sediment transport, sea-level rise, monsoonal processes, coastal protection, mangrove

restoration and human activity (Chawalit *et al.,* 2025). These comparisons suggest that Cirebon should not be interpreted as a uniformly eroding or accreting coast, but as a spatially heterogeneous coastal system where localized hotspots are especially important for salt-farming exposure.

In the context of salt farming, the main implication is that operational exposure may arise from a limited number of shoreline sectors, even when the broader coastline appears accretion-dominant by transect count. This is consistent with empirical work from northern Java which showed that coastal hazards and shoreline instability could place operational stress on salt-production landscapes, including pond-boundary disturbance, access disruption and changes in management routines (Nirwansyah & Braun, 2019, 2021a; Sutrisno *et al.,* 2021). However, the impact framework developed here should be interpreted as a remote-sensing-based screening tool rather than direct evidence of confirmed salt-pan damage. The categories identify where shoreline dynamics may intersect with salt-farming infrastructure, but they do not directly measure embankment failure, yield reduction, repair costs, maintenance frequency or impacts on household livelihoods. This distinction is important because field validation, farmer interviews, production records and historical photographs of affected salt pans were not available for the full multi-decadal period. Therefore, the most feasible interpretation is that EPR, NSM and SCE identify potential exposure pathways between shoreline dynamics and salt-pan infrastructure, but not confirmed economic loss or observed operational failure.

Thematically, the study contributes an operational workflow that links cloud-based multi-decadal shoreline extraction and preprocessing with QSCAT transect statistics, establishing a repeatable basis for shoreline-change assessment in settings where consistent long-term monitoring is limited (Gómez-Pazo *et al.,* 2021; Tang *et al.,* 2023; Yasir *et al.,* 2020). A second contribution is the use of multiple complementary metrics rather than reliance on a single rate indicator. The combined interpretation of EPR, NSM and SCE allows the analysis to distinguish between shoreline direction, cumulative displacement, and positional variability.

This is important for salt farming because large-scale cumulative displacement and wide shoreline envelopes may indicate locations where pond boundaries, intake channels, drainage routes and access paths are more likely to require adjustment. Similar studies in Southeast Asia also demonstrate the value of using multi-temporal satellite imagery and shoreline-change tools such as DSAS/QSCAT to quantify long-term coastal dynamics and identify hotspots for coastal management (Abd-Elhamid *et al.,* 2023; Chawalit *et al.,* 2025; Pantusa *et al.,* 2022; Quang *et al.,* 2021). However, this study differs from many previous shoreline-monitoring ones by translating physical shoreline-change metrics into salt-farming-relevant exposure categories (Pantusa *et al.,* 2022; Tang *et al.,* 2023). This helps address a gap in the literature, where shoreline change is often mapped as a physical process, but is less frequently connected to livelihood-specific infrastructure such as salt pans, bunds, seawater-intake channels and access routes.

Several limitations and uncertainties should guide interpretation of the study findings. First, because high-resolution elevation, complete tidal-stage information, and field-based inundation data were not available, high-change categories should be interpreted as shoreline-instability exposure proxies rather than direct inundation-risk classes. This restricts conclusions about flooding frequency, overtopping thresholds or depth of inundation in salt pans. Second, as in other multi-decadal optical shoreline studies, the results are sensitive to shoreline-proxy definition, water-level differences between image dates, sensor resolution, georeferencing uncertainty, and mixed land-water pixels. These factors may inflate apparent variability when shoreline changes are small, which is why this study uses uncertainty-aware interpretation and emphasizes spatially coherent patterns rather than isolated transect-level patterns ones (Abd-Elhamid *et al.,* 2023; Gómez-Pazo *et al.,* 2021; Jayanthi *et al.,* 2023; Pantusa *et al.,* 2022).

Third, the selected epochs of 1995, 2005, 2015 and 2025 were designed to capture net decadal shoreline change, not annual or event-scale variability. The 2015–2025 period should therefore be understood as one of net-change; shorter-term erosion, accretion, storm-driven change or temporary recovery within that decade may not be fully captured. Fourth, while the analysis identifies where shoreline dynamics are strongest, it does not quantify salt-production loss, repair costs, intervention frequency or household-level impacts. Future work should combine category-coded transects with parcel-level salt-pan boundaries, UAV or drone surveys, GPS mapping of embankments and intake channels, participatory mapping with salt farmers, farmer interviews, production records, and maintenance-cost documentation. This would allow related research to move from identifying potential exposure towards measuring actual operational and socioeconomic impacts.

4. Conclusion

The study demonstrates that multi-decadal shoreline analysis can support exposure screening for salt-farming landscapes in Cirebon, West Java. By integrating satellite-derived shoreline positions, QSCAT-based shoreline-change metrics, and salt-farming exposure interpretation, spatially uneven shoreline dynamics are identified, where accretion-dominant transect counts coexist with localized erosion hotspots. This pattern shows that coastline-wide summaries alone may obscure critical local instability, especially where a relatively small number of high-magnitude retreat segments strongly influence overall shoreline-change signals. For salt-farming systems, these localized high-change areas are important because they may indicate zones where shoreline insta bility could affect salt-pan boundaries, embankments, access routes, seawater-intake channels, drainage systems and sediment-management routines. The study therefore contributes to coastal vulnerability research by translating EPR, NSM, LRR and SCE metrics into salt-farming-relevant exposure pathways, rather than treating shoreline movement only as a physical coastal process. This sector-specific interpretation is particularly relevant for Global South coastal settings, where long-term field monitoring is often limited, but livelihood dependence on low-lying coastal production systems remains high.

Acknowledgements

The research received partial funding from Universitas Muhammadiyah Purwokerto (UMP) through their International Collaborative Program (KLN) Batch 2, in partnership with Ataturk University, Turkey and Mahidol University, Thailand. All the authors contributed equally to the writing process. They would like to thank the reviewers for their valuable feedback and comments, which have enhanced the quality of the article.

Author Contributions

Conceptualization: Nirwansyah, A. W., Hakim, D. K., Andriani, A., Demirdag, I., & Rana, S.; **methodology**: Nirwansyah, A. W., Hakim, D. K., Andriani, A., Demirdag, I., & Rana, S.; **investigation**: Nirwansyah, A. W., Hakim, D. K., Andriani, A., Demirdag, I., & Rana, S.; **writing—original draft preparation**: Nirwansyah, A. W., Hakim, D. K., Andriani, A., Demirdag, I., & Rana, S.; **writing—review and editing**: Nirwansyah, A. W., Hakim, D. K., Andriani, A., Demirdag, I., & Rana, S.; **visualization**: Nirwansyah, A. W., Hakim, D. K., Andriani, A., Demirdag, I., & Rana, S.. All authors have read and agreed to the published version of the manuscript.

Conflict of interest

All authors declare that they have no conflicts of interest.

Data availability

Data is available upon Request.

Funding

The research funds were made available through Budget Year 2025, grant Number: A.11-III/7958-S.Pj./LPPM/III/2025

References

Abd-Elhamid, H. F., Zeleňáková, M., Barańczuk, J., Gergeľová, M. B., & Mahdy, M. (2023). Historical Trend Analysis and Forecasting of Shoreline Change at the Nile Delta Using RS Data and GIS With the DSAS Tool. *Remote Sensing*, 15(7), 1737. doi: 10.3390/rs15071737

Adnan, M. S. G., Abdullah, A. Y. M., Dewan, A., & Hall, J. W. (2020). The effects of changing land use and flood hazard on poverty in coastal Bangladesh. *Land Use Policy*, 99, 104868. doi: 10.1016/j.landusepol.2020.104868

Al-Ali, Z., Abulibdeh, A., Al-Awadhi, T., Mohan, M., Al Nasiri, N., Al-Barwani, M., Al Nabbi, S., & Abdullah, M. (2024). Examining the potential and effectiveness of water indices using multispectral sentinel-2 data to detect soil moisture as an indicator of mudflow occurrence in arid regions. *International Journal of Applied Earth Observation and Geoinformation*, 130, 103887. doi: 10.1016/j.jag.2024.103887

Anderson, C. C., Renaud, F. G., Hagenlocher, M., & Day, J. W. (2021). Assessing multi-hazard vulnerability and dynamic coastal flood risk in the Mississippi Delta: The global delta risk index as a social-ecological systems approach. *Water (Switzerland)*, 13(4). doi: 10.3390/w13040577

Anugrah, R. D., & Setiawati, M. D. (2022). Integrated Study on Tsunami Impact Assessment in Cilacap, Indonesia: Method, Approach, and Practice. *Springer Climate*, 577–605. doi: 10.1007/978-3-031-15501-7_23

Apostolopoulos, D. N., & Nikolakopoulos, K. G. (2020). Assessment and quantification of the accuracy of low-and high-resolution remote sensing data for shoreline monitoring. *ISPRS International Journal of Geo-Information*, 9(6). doi: 10.3390/ijgi9060391

Arjasakusuma, S., Kusuma, S. S., Saringatin, S., Wicaksono, P., Mutaqin, B. W., & Rafif, R. (2021). Shoreline dynamics in East Java Province, Indonesia, from 2000 to 2019 using multi-sensor remote sensing data. *Land*, 10(2), 1–17. doi: 10.3390/land10020100

Badriana, M. R., Abdurrahman, U., Arifin Nur, A., Jeon, C., Miliachristi Radjawane, I., & Park, H. (2024). Tidal Characteristic Analysis Utilizing Radar Tide Gauge in Cirebon Seawater. *Jurnal Ilmu Dan Teknologi Kelautan Tropis*, 16(1), 105–115. doi: 10.29244/jitkt.v16i1.52987

Bagheri-Gavkosh, M., Hosseini, S. M., Ataie-Ashtiani, B., Sohani, Y., Ebrahimian, H., Morovat, F., & Ashrafi, S. (2021). Land subsidence: A global challenge. *Science of the Total Environment*, 778. doi: 10.1016/j.scitotenv.2021.146193

Baig, M. R. I., Shahfahad, Ahmad, I. A., Tayyab, M., Asgher, M. S., & Rahman, A. (2021). Coastal Vulnerability Mapping by Integrating Geospatial Techniques and Analytical Hierarchy Process (AHP) along the Vishakhapatnam Coastal Tract, Andhra Pradesh, India. *Journal of the Indian Society of Remote Sensing*, 49(2), 215–231. doi: 10.1007/s12524-020-01204-6

Bramanto, B., Gumilar, I., Sidiq, T. P., Rahmawan, Y. A., & Abidin, H. Z. (2023). Geodetic evidence of land subsidence in Cirebon, Indonesia. *Remote Sensing Applications: Society and Environment*, 30, 100933. doi: 10.1016/j.rsase.2023.100933

Bushra, N., Mostafiz, R. Bin, Rohli, R. V., Friedland, C. J., & Rahim, M. A. (2021). Technical and Social Approaches to Study Shoreline Change of Kuakata, Bangladesh. *Frontiers in Marine Science*, 8, 1–13. doi: 10.3389/fmars.2021.730984

Cai, S., Fan, J., & Yang, W. (2021). Flooding risk assessment and analysis based on gis and the tfn-ahp method: A case study of chongqing, china. *Atmosphere*, 12(5). doi: 10.3390/atmos12050623

Chakma, P., & Akter, A. (2021). Flood Mapping in the Coastal Region of Bangladesh Using Sentinel-1 SAR Images: A Case Study of Super Cyclone Amphan. *Journal of the Civil Engineering Forum*, 7(3), 267. doi: 10.22146/jcef.64497

Chander, G., Markham, B. L., & Barsi, J. A. (2007). Revised Landsat-5 Thematic Mapper Radiometric Calibration. *IEEE Geoscience and Remote Sensing Letters*, 4(3), 490–494. doi: 10.1109/LGRS.2007.898285

Chander, G., Markham, B. L., & Helder, D. L. (2009). Summary of current radiometric calibration coefficients for Landsat MSS, TM, ETM+, and EO-1 ALI sensors. *Remote Sensing of Environment*, 113(5), 893–903. doi: 0.1016/j.rse.2009.01.007

Chawalit, C., Boonpook, W., Sitthi, A., Torsri, K., Kamthonkiat, D., Tan, Y., Suwansaard, A., & Nardkulpat, A. (2025). Geoinformatics and Machine Learning for Shoreline Change Monitoring: A 35-Year Analysis of Coastal Erosion in the Upper Gulf of Thailand. *ISPRS International Journal of Geo-Information*, 14(2). doi: 10.3390/ijgi14020094

Chung, S., Takeuchi, J., Fujihara, M., & Oeurng, C. (2019). Flood damage assessment on rice crop in the Stung Sen River Basin of Cambodia. *Paddy and Water Environment*, 17(2), 255–263. doi: 10.1007/s10333-019-00718-1

Ciritci, D., & Türk, T. (2019). Automatic Detection of Shoreline Change by Geographical Information System (GIS) and Remote Sensing in the Göksu Delta, Turkey. *Journal of the Indian Society of Remote Sensing*, 47(2), 233–243. doi: 10.1007/s12524-019-00947-1

Dewa, H. P. N., Nirwansyah, A. W., Dewi, R. S., & Demirdag, I. (2023). Vulnerability Analysis of School Buildings to Tsunami in the Cilacap Coastal Area. *Forum Geografi*, 37(2). doi: 10.23917/forgeo.v37i2.23269

Dewi, R. S., & Bijker, W. (2020). Dynamics of shoreline changes in the coastal region of Sayung, Indonesia. *Egyptian Journal of Remote Sensing and Space Science*, 23(2), 181–193. doi: 10.1016/j.ejrs.2019.09.001

Dewidar, K., & Bayoumi, S. (2021). Forecasting shoreline changes along the Egyptian Nile Delta coast using Landsat image series and Geographic Information System. *Environmental Monitoring and Assessment*, 193(7), 1–11. doi: 10.1007/s10661-021-09192-x

Dhanalakshmi, S., Kankara, R. S., & Chenthamil Selvan, S. (2019). Impact assessment of sea level rise over coastal landforms: a case study of Cuddalore coast, south-east coast of India. *Environmental Earth Sciences*, 78(16), 1–14. doi: 10.1007/s12665-019-8463-1

Ekrami, J., Nemati Mansour, S., Mosaferi, M., & yamini, Y. (2021). Environmental impact assessment of salt harvesting from the salt lakes. *Journal of Environmental Health Science and Engineering,* 19(1), 365-377. doi: 10.1007/s40201-020-00609-2

Elnabwy, M. T., Elbeltagi, E., El Banna, M. M., Elshikh, M. M. Y., Motawa, I., & Kaloop, M. R. (2020). An approach based on landsat images for shoreline monitoring to support integrated coastal management - A case study, ezbet elborg, nile delta, Egypt. *ISPRS International Journal of Geo-Information*, 9(4). doi: 10.3390/ijgi9040199

Facun, L. P., Sta Maria, M. Y., Ducao, R., Clemente, J. J., Carmelo, E. M., Maon, A., Malaya, A. R., Cuison, F., & Siringan, F. (2025). QGIS Shoreline Change Analysis Tool (QSCAT): A fast, open-source shoreline change analysis plugin for QGIS. *Environmental Modelling & Software*, 184, 106263. doi: 10.1016/j.envsoft.2024.106263

Fathurrahman, F., Mubarak, M., Nurrachmi, I., Rifardi, R., & Ilahi, I. (2025). Study of Waves, Currents and Coastline Changes in North Rupat Sub-District, Bengkalis Regency, Riau. *Jurnal Natur Indonesia*, 23(1), 42–49. doi: 10.31258/jnat.23.1.42-49

Galan, J. P. B., Gonzales, D. D. O., Tamondong, A. M., & Quiros, A. L. (2026). Assessing the Relationship between Coastal Reclamation and Seagrass Ecosystems in Coron, Palawan using Multitemporal Remote Sensing, Shoreline Change Analysis, and Turbidity Mapping. *ISPRS Annals of the Photogrammetry, Remote Sensing and Spatial Information Sciences*, 10(5-W4-2025), 253–260. doi: 10.5194/isprs-annals-X-5-W4-2025-253-2026

Gallina, V., Torresan, S., Zabeo, A., Critto, A., Glade, T., & Marcomini, A. (2020). A Multi-Risk Methodology for the Assessment of Climate Change Impacts in Coastal Zones. *Sustainability*, 12(9), 3697. doi: 10.3390/su12093697

Glavan, M., Cvejić, R., Zupanc, V., Knapič, M., & Pintar, M. (2020). Agricultural production and flood control dry detention reservoirs: Example from Lower Savinja Valley, Slovenia. *Environmental Science and Policy*, 114, 394–402. doi: 10.1016/j.envsci.2020.09.012

Gómez-Pazo, A., Payo, A., Paz-Delgado, M. V, & Delgadillo-Calzadilla, M. A. (2021). Open Digital Shoreline Analysis System: ODSAS v1.0. *Journal of Marine Science and Engineering*, 10(1), 26. doi: 10.3390/jmse10010026

Hossain, A., Krupnik, T. J., Timsina, J., Mahboob, M. G., Chaki, A. K., Farooq, M., Bhatt, R., Fahad, S., & Hasanuzzaman, M. (2020). Agricultural Land Degradation: Processes and Problems Undermining Future Food Security. In *Environment, Climate, Plant and Vegetation Growth,* 17–61. doi: 10.1007/978-3-030-49732-3_2

Huang, X., Fu, Y., Ding, H., Tang, G., Ma, P., Liu, L., Xue, Y., Wu, S., & Chen, Y. (2025). Inter-annual changes and growth trends mapping of mangrove using Landsat time series imagery. *GIScience and Remote Sensing*, 62(1). doi: 10.1080/15481603.2025.2480422

Illigner, J., Haghshenas, M., Gisevius, K., & Braun, B. (2021). Land subsidence in Jakarta and Semarang Bay–The relationship between physical processes, risk perception, and household adaptation. *Ocean & Coastal Management,* 211, 105775. doi: 10.1016/j.ocecoaman.2021.105775

Islam, M. R., & Raja, D. R. (2021). Waterlogging Risk Assessment: An Undervalued Disaster Risk in Coastal Urban Community of Chattogram, Bangladesh. *Earth (Switzerland)*, 2(1), 151–173. doi: 10.3390/earth2010010

Jayanthi, M., Duraisamy, M., Kabiraj, S., Thirumurthy, S., Samynathan, M., Panigrahi, A., & Muralidhar, M. (2022). Are the Sundarbans, the World's Largest Mangroves Region Under Threat?—An Ecosystem-based Geospatial Approach to Assess Changes Past, Present, and Future in Relation to Natural and Human-induced Factors. *Land Degradation and Development*, 34(1), 125–141. doi: 10.1002/ldr.4448

Jayanthi, M., Duraisamy, M., Kabiraj, S., Thirumurthy, S., Samynathan, M., Panigrahi, A., Muralidhar, M., Mageswaran, T., Sachithanandam, V., Sridhar, R., Mahapatra, M., Ramesh, R., Phan, M. H., Stive, M. J. F., Zoysa, S. D., Basnayake, V., Samarasinghe, J. T., Gunathilake, M. B., Kantamaneni, K., … Windupranata, W. (2023). Monitoring of Coastal Dynamics at Subang Regency Using Landsat Collection Data and Cloud Computing Based. *Water*, 15(1), 176. doi: 10.1002/esp.5522

Kantamaneni, K., Rice, L., Yenneti, K., & Campos, L. C. (2020). Assessing the vulnerability of agriculture systems to climate change in coastal areas: A novel index. *Sustainability (Switzerland)*, 12(11). doi: 10.3390/su12114771

Kumar, P., Debele, S. E., Sahani, J., Rawat, N., Marti-Cardona, B., Alfieri, S. M., Basu, B., Basu, A. S., Bowyer, P., Charizopoulos, N., Gallotti, G., Jaakko, J., Leo, L. S., Loupis, M., Menenti, M., Mickovski, S. B., Mun, S. J., Gonzalez-Ollauri, A., Pfeiffer, J., … Zieher, T. (2021). Nature-based solutions efficiency evaluation against natural hazards: Modelling methods, advantages and limitations. *Science of the Total Environment*, 784. doi: 10.1016/j.scitotenv.2021.147058

Liang, H., & Zhou, X. (2022). Impact of Tides and Surges on Fluvial Floods in Coastal Regions. *Remote Sensing*, 14(22), 1–17. doi: 10.3390/rs14225779

Lizcano-Sandoval, L., Anastasiou, C., Montes, E., Raulerson, G., Sherwood, E., & Muller-Karger, F. E. (2022). Seagrass distribution, areal cover, and changes (1990–2021) in coastal waters off West-Central Florida, USA. *Estuarine, Coastal and Shelf Science*, 279, 108134. doi: 10.1016/j.ecss.2022.108134

Mageswaran, T., Sachithanandam, V., Sridhar, R., Mahapatra, M., & Ramesh, R. (2021). Impact of Sea Level Rise and Shoreline Changes in the Tropical Island Ecosystem of Andaman and Nicobar Region, India. *Natural Hazards*, 109(2), 1717–1741. doi: 10.1007/s11069-021-04895-3

Makris, C., Mallios, Z., Androulidakis, Y., & Krestenitis, Y. (2023). CoastFLOOD: A High-Resolution Model for the Simulation of Coastal Inundation Due to Storm Surges. *Hydrology*, 10(5). doi: 10.3390/hydrology10050103

Manurung, R. F. P., Khakhim, N., & Susilo, B. (2025). Quantify Relation of SLR and Changes Along Karawang Coastal: GIS and Statistical Model Utilization. *IOP Conference Series: Earth and Environmental Science*, 1503(1). doi: 10.1088/1755-1315/1503/1/012030

McClenachan, G., Donnelly, M. J., Shaffer, M., Sacks, P., & Walters, L. J. (2020). Does Size Matter? Quantifying the Cumulative Impact of Small-scale Living Shoreline and Oyster Reef Restoration Projects on Shoreline Erosion. *Restoration Ecology*, 28(6), 1365–1371. doi: 10.1111/rec.13235

Meister, M., & Qu, J. J. (2024). Quantifying Seagrass Density Using Sentinel-2 Data and Machine Learning. *Remote Sensing*, 16(7), 1–19. doi: 10.3390/rs16071165

Muskananfola, M. R., Supriharyono, & Febrianto, S. (2020). Spatio-temporal analysis of shoreline change along the coast of Sayung Demak, Indonesia using Digital Shoreline Analysis System. *Regional Studies in Marine Science*, 34, 101060. doi: 10.1016/j.rsma.2020.101060

Nirwansyah, A. W., & Braun, B. (2019). Mapping Impact of Tidal Flooding on Solar Salt Farming in Northern Java using a Hydrodynamic Model. *ISPRS International Journal of Geo-Information*, 8(10), 451. doi: 10.3390/ijgi8100451

Nirwansyah, A. W., & Braun, B. (2021a). Assessing the degree of tidal flood damage to salt harvesting landscape using synthetic approach and GIS - Case study: Cirebon, West Java. *International Journal of Disaster Risk Reduction*, 55, 102099. doi: 10.1016/j.ijdrr.2021.102099

Nirwansyah, A. W., & Braun, B. (2021b). Tidal Flood Risk on Salt Farming: Evaluation of Post Events in the Northern Part of Java Using a Parametric Approach. *Geosciences*, 11(10), 420. doi: 10.3390/geosciences11100420

Nirwansyah, A. W., Braun, B., Demirdag, I., & Suwarno. (2023). Method for economic loss estimation in traditional coastal salt farming towards tidal inundation. *MethodsX*, 10, 102176. doi: 10.1016/j.mex.2023.102176

Nirwansyah, A. W., Braun, B., & Ramdani, F. (2022). Salt for living: sustainable practice of salt harvesting in the Cirebonese community and its threat by coastal hazard. In *Indigenous People and Nature*, 577-592. doi: 10.1016/B978-0-323-91603-5.00006-3

Pantusa, D., D'Alessandro, F., Frega, F., Francone, A., & Tomasicchio, G. R. (2022). Improvement of a Coastal Vulnerability Index and Its Application Along the Calabria Coastline, Italy. *Scientific Reports*, 12(1). doi: 10.1038/s41598-022-26374-w

Pelckmans, I., Belliard, J.-P., Dominguez-Granda, L. E., Slobbe, C., Temmerman, S., & Gourgue, O. (2023). Mangrove ecosystem properties regulate high water levels in a river delta. *Natural Hazards and Earth System Sciences*, 23(9), 3169–3183. doi: 10.5194/nhess-23-3169-2023

Phan, M. H., & Stive, M. J. F. (2022). Managing Mangroves and Coastal Land Cover in the Mekong Delta. *Ocean & Coastal Management*, 219, 106013. doi: 10.1016/j.ocecoaman.2021.106013

Quang, D. N., Ngan, V. H., Tam, H. S., Viet, N. T., Tinh, N. X., & Tanaka, H. (2021). Long-term shoreline evolution using dsas technique: A case study of Quang Nam province, Vietnam. *Journal of Marine Science and Engineering*, 9(10). doi: 10.3390/jmse9101124

Roy, D. P., Wulder, M. A., Gorelick, N., Hansen, M., Healey, S., Hostert, P., Huntington, J., Radeloff, V. C., Scambos, T., Schaaf, C., Woodcock, C. E., & Zhu, Z. (2026). The next Landsat: Mission turning point? *Remote Sensing of Environment*, 332, 115087. doi: 10.1016/j.rse.2025.115087

Rutkayová, J., Vácha, F., Maršálek, M., Beneš, K., Civišová, H., Horká, P., Petrášková, E., Rost, M., & Šulista, M. (2018). Fish stock losses due to extreme floods - findings from pond-based aquaculture in the Czech Republic. *Journal of Flood Risk Management*, 11(3), 351–359. doi: 10.1111/jfr3.12332

Salik, K. M., Jahangir, S., Zahdi, W. ul Z., & Hasson, S. ul. (2015). Climate change vulnerability and adaptation options for the coastal communities of Pakistan. *Ocean & Coastal Management*, 112, 61–73. doi: 10.1016/j.ocecoaman.2015.05.006

Shamsuzzoha, M., & Ahamed, T. (2023). Shoreline Change Assessment in the Coastal Region of Bangladesh Delta Using Tasseled Cap Transformation From Satellite Remote Sensing Dataset. *Remote Sensing*, 15(2), 295. doi: 10.3390/rs15020295

Shokoohi, A., Ganji, Z., Samani, J. M. V., & Singh, V. P. (2018). Analysis of spatial and temporal risk of agricultural loss due to flooding in paddy farms. *Paddy and Water Environment*, 16(4), 737–748. doi: 10.1007/s10333-018-0665-8

Solihuddin, T., Husrin, S., Salim, H. L., Kepel, T. L., Mustikasari, E., Heriati, A., Ati, R. N. A., Purbani, D., Mbay, L. O. N., Indriasari, V. Y., & Berliana, B. (2021). Coastal erosion on the north coast of Java: Adaptation strategies and coastal management. *IOP Conference Series: Earth and Environmental Science*, 777(1). doi: 10.1088/1755-1315/777/1/012035

Stelten, R., & Antczak, K. A. (2022). Life at the Salty Edge of Empire : The Maritime Cultural Landscape at the Orange Saltpan on Bonaire , 1821 – 1960. In *International Journal of Historical Archaeology*, 0123456789. doi: 10.1007/s10761-022-00660-9

Sunny, D. S., Islam, K. M. A., Mullick, M. R. A., & Ellis, J. T. (2022). Performance study of imageries from MODIS, Landsat 8 and Sentinel-2 on measuring shoreline change at regional scale. *Remote Sensing Applications: Society and Environment*, 28, 100816. doi: 10.1016/j.rsase.2022.100816

Susantoro, T. M., Wikantika, K., Yayusman, L. F., Tan, A., & Ghozali, M. F. (2020). Monitoring of Mangrove Growth and Coastal Changes on the North Coast of Brebes, Central Java, Using Landsat Data. *International Journal of Remote Sensing and Earth Sciences (IJReSES)*, 16(2), 197. doi: 10.30536/j.ijreses.2019.v16.a3221

Sutrisno, D., Darmawan, M., Rahadiati, A., Helmi, M., Yusmur, A., Hashim, M., Shih, P. T. Y., Qin, R., & Zhang, L. (2021). Spatial-planning-based ecosystem adaptation (SPBEA): A concept and modeling of prone shoreline retreat areas. *ISPRS International Journal of Geo-Information*, 10(3). doi: 10.3390/ijgi10030176

Tang, W., Hearne, H. S., Slocum, Z., & Chen, T. (2023). GIS-Based Scientific Workflows for Automated Spatially Driven Sea Level Rise Modeling. *Sustainability*, 15(17), 12704. doi: 10.3390/su151712704

Traganos, D., Aggarwal, B., Poursanidis, D., Topouzelis, K., Chrysoulakis, N., & Reinartz, P. (2018). Towards global-scale seagrass mapping and monitoring using Sentinel-2 on Google Earth Engine: The case study of the Aegean and Ionian Seas. *Remote Sensing*, 10(8), 1–14. doi: 10.3390/rs10081227

van Bijsterveldt, C. E. J., Debrot, A. O., Bouma, T. J., Maulana, M. B., Pribadi, R., Schop, J., Tonneijck, F. H., & van Wesenbeeck, B. K. (2022). To Plant or Not to Plant: When can Planting Facilitate Mangrove Restoration? *Frontiers in Environmental Science*, 9, 1–18. doi: 10.3389/fenvs.2021.690011

van Hespen, R., Hu, Z., Borsje, B., De Dominicis, M., Friess, D. A., Jevrejeva, S., Kleinhans, M. G., Maza, M., van Bijsterveldt, C. E. J., Van der Stocken, T., van Wesenbeeck, B., Xie, D., & Bouma, T. J. (2023). Mangrove forests as a nature-based solution for coastal flood protection: Biophysical and ecological considerations. *Water Science and Engineering*, 16(1), 1–13. doi: 10.1016/j.wse.2022.10.004

Wang, W., Zaheer, Q., Qiu, S., Wang, W., Ai, C., Wang, J., Wang, S., & Hu, W. (2023). *Digital Twin Technologies in Transportation Infrastructure Management.* Digital Twin Technologies in Transportation Infrastructure Management. doi: 10.1007/978-981-99-5804-7

Wisha, U. J., Dhiauddin, R., Ondara, K., Gemilang, W. A., & Rahmawan, G. A. (2022). Assessing Urban Development Impacts in the Padang Coastline City, West Sumatra Indonesia; Coastline Changes and Coastal Vulnerability. *Geoplanning*, 9(2), 73–88. doi: 10.14710/geoplanning.9.2.73-88

Yasir, M., Sheng, H., Fan, H., Nazir, S., Niang, A. J., Salauddin, M., & Khan, S. (2020). Automatic Coastline Extraction and Changes Analysis Using Remote Sensing and GIS Technology. *IEEE Access*, 8, 180156–180170. doi: 10.1109/ACCESS.2020.3027881

Yulfa, A., Chandra, D., Ramadhan, R., & Andreas, A. (2022). Geovisualization for information extraction of shoreline changes in Padang city 2000–2020. *Geodesy and Cartography (Vilnius)*, 48(2), 78–84. doi: 10.3846/gac.2022.14212

Yuwono, B. D., Abidin, H. Z., Poerbandono, Andreas, H., Pratama, A. S. P., & Gradiyanto, F. (2024). Mapping of flood hazard induced by land subsidence in Semarang City, Indonesia, using hydraulic and spatial models. *Natural Hazards*, 120(6), 5333–5368. doi: 10.1007/s11069-023-06398-9

Zhang, H. K., & Roy, D. P. (2016). Computationally inexpensive Landsat 8 Operational Land Imager (OLI) pansharpening. *Remote Sensing*, 8(3), 1–25. doi: 10.3390/rs8030180

Zoysa, S. D., Basnayake, V., Samarasinghe, J. T., Gunathilake, M. B., Kantamaneni, K., Muttil, N., Pawar, U., & Rathnayake, U. (2023). Analysis of Multi-Temporal Shoreline Changes Due to a Harbor Using Remote Sensing Data and GIS Techniques. *Sustainability*, 15(9), 7651. doi: 10.3390/su15097651